Chapter 4

Fokker-Planck equations for IP_3 mediated Ca^{2+} dynamics

4.1 Introduction

Modeling the dynamics of intracellular calcium released through IP_3 receptor channels has proceeded along two roads in the past: deterministic approaches (De Young and Keizer 1992, Li and Rinzel 1994, Sneyd and Tsaneva-Atanasova 2003) and stochastic methods (Falcke et al. 2000b, Falcke 2003b, Shuai and Jung 2002b, Meinhold and Schimansky-Geier 2002). Deterministic models have been successfully applied to study intracellular wave phenomena such as fertilization waves or the impact of mitochondria on waves. For a recent review see (Falcke 2004). However, stochastic simulations have revealed that fluctuations originating from the binding and unbinding of molecules to the IP_3 receptor have to be taken into account. That was again demonstrated by the results of chapter 2. We here propose a master equation and corresponding Fokker-Planck equations to further clarify the effects of fluctuations on intracellular Ca^{2+} dynamics.

The reason why fluctuations must not be neglected for IP_3 induced Ca^{2+} dynamics lies in their ability to induce oscillations of the Ca^{2+} concentration. Deterministic models with realistic m parameters are either monostable or possess an oscillatory regime that is too small to be of experimental importance (Thul and Falcke 2005, Thul and Falcke 2004b). Hence, noise can lead to dynamical regimes that are absent without it. Such a behavior has been already observed in different fields. Fronts that are stable without fluctuations undergo a diffusive instability (Kessler and Levine 1998), or patterns emerge that do not occur without fluctuations (Vilar and Rubí 1997, Zaikin et al. 2002, Togashi and Kaneko 2004). Consequently, fluctuations essentially shape the dynamics of a system.

In the case of intracellular Ca^{2+}, the role of oscillations is pivotal to a cell. It is one of the means with which it controlls metabolism or gene expression. Understanding the mechanisms that lead to these oscillations is therefore of significant interest. For the time being no final consensus has been achieved about these processes. One way to envisage Ca^{2+} oscillations is as follows. We start with a group of IP_3 receptor clusters. In the course of time a puff raises the Ca^{2+} concentration at a single cluster. It causes an elevation of the Ca^{2+} concentration at neighboring clusters. The open probability at these clusters grows. This may induce channel opening, but it does not have to. If none of the surrounding clusters open, the puff remains an isolated event. A completely different scenario occurs as soon as more clusters open. The Ca^{2+} concentration increases to such an extent at the neighboring clusters that it is very likely for them to open as well. It causes a further elevation of the Ca^{2+} concentration which can lead to additional open clusters. This is the beginning of one Ca^{2+} oscillation. Continuing this process leads to a Ca^{2+} wave which travels through a cell or only through parts of it.

The quantity that decides whether a Ca^{2+} liberation stays localized or spreads through a larger area is the number of clusters that open in a small region within a short time. If too little clusters are involved, the Ca^{2+} concentration does not grow sufficiently enough at the adjacent clusters to induce a high opening probability. A minimal number of open clusters is required for this. Picturing them as a group they represent a nucleus from which a Ca^{2+} wave starts. Hence, there exists a critical nucleus for Ca^{2+} oscillations.

The period of these oscillations may be decomposed into a stochastic and a deterministic part. Stochasticity enters via the time to form the critical nucleus. There is only a certain probability that a puff opens neighboring clusters. Once the clusters are open, the high Ca^{2+} concentration inhibits all channels. Inhibition and recovery from it constitute the deterministic fraction of the period. Stochastic simulations have shown that long period oscillations are controlled by the nucleation probability, whereas short periods can be explained by the time scale of inhibition and recovery (Falcke 2003b).

The above separation of the period does not only hold for Ca^{2+} oscillations, but also for the localized Ca^{2+} puffs. The deterministic part corresponds again to inhibition and recovery from it. The interpretation of the stochastic fraction changes. In this chapter we will address it more closely. We will provide tools to estimate the stochastic part of the puff period because puffs are the basic building blocks of intracellular Ca^{2+} dynamics.

4.2 The master equation

We saw in section 3.3 that the state of an IP_3 receptor is determined by the state of its subunits. Therefore a single subunit acts as the basic building block of the receptor's dynamics. Considering a cluster of IP_3Rs this picture remains valid. Let n_i denote the number of subunits in the state i. Then the dynamics of the cluster is governed by the time evolution of each n_i. The discussion in section 3.3 already suggests that this process is most conveniently described by a master equation. Hence we study the probability $P(\{n_i\})$ for a given configuration $\{n_i\}$. The precise form of the master equation depends on the state scheme for the IP_3 receptor. We here apply the state scheme depicted in figure 3.4. Consequently, we characterize the cluster by the number of activable subunits n_{10}, the number of inhibited subunits $n_{\bar{h}}$ and the number of subunits with no Ca^{2+} bound n_{00}. We will study a cluster consisting of N channels with h subunits each. Hence, the total number of subunits is fixed to $Nh = n_{10} + n_{\bar{h}} + n_{00}$. This relation allows to concentrate on the two variables n_{10} and $n_{\bar{h}}$ only. The value of n_{00} is uniquely determined by the above sum. Consequently, the probability to find a configuration $(n_{10}, n_{\bar{h}}, n_{00})$ is identical to the probability $P(n_{10}, n_{\bar{h}})$ for the set $(n_{10}, n_{\bar{h}})$. Its time evolution is governed by the master equation

$$\begin{aligned}
\dot{P}(n_{10}, n_{\bar{h}}) = &- [n_{10}(b_5 + a_6 c(n_{10})) + n_{\bar{h}} b_6]\, P(n_{10}, n_{\bar{h}}) \\
&- [hN - n_{10} - n_{\bar{h}}][a_5 c(n_{10}) + a_6 c(n_{10})] P(n_{10}, n_{\bar{h}}) \\
&+ [hN - n_{\bar{h}} - (n_{10} - 1)] a_5 c(n_{10} - 1) P(n_{10} - 1, n_{\bar{h}}) \\
&+ [hN - n_{\bar{h}} - (n_{10} - 1)] a_6 c(n_{10}) P(n_{10}, n_{\bar{h}} - 1) \\
&+ [n_{10} + 1] a_6 c(n_{10} + 1) P(n_{10} + 1, n_{\bar{h}} - 1) \\
&+ [n_{10} + 1] b_5 P(n_{10} + 1, n_{\bar{h}}) \\
&+ \frac{b_6 c(n_{10} - 1)}{c(n_{10} - 1) + d_5} (n_{\bar{h}} + 1) P(n_{10} - 1, n_{\bar{h}} + 1) \\
&+ \frac{b_6 d_5}{c(n_{10}) + d_5} (n_{\bar{h}} + 1) P(n_{10}, n_{\bar{h}} + 1)\,.
\end{aligned} \tag{4.1}$$

The first two lines describe the loss processes from the state $(n_{10}, n_{\bar{h}})$. Being in $(n_{10}, n_{\bar{h}})$ the terms $n_{10} b_5$ and $n_{10} a_6 c(n_{10})$ denote the transitions from 10 to 00 and to $\bar{h}$, respectively. Hence n_{10} changes to $n_{10} - 1$ and n_{00} as well as $n_{\bar{h}}$ to $n_{00} + 1$ and $n_{\bar{h}} + 1$, respectively. Although the probability in equation (4.1) only takes n_{10} and $n_{\bar{h}}$ as arguments, we still have to include the transitions involving n_{00}. The

rate $n_{\bar{h}} b_6$ subsumes the transitions from $\bar{h}$ to 10 and 00, whereas the second line governs the transitions from 00. The remaining lines control the gain processes into the state $(n_{10}, n_{\bar{h}})$. For instance $(n_{10}+1)b_{\bar{5}}$ is the rate for going from the state $(n_{10}+1, n_{\bar{h}})$ into $(n_{10}, n_{\bar{h}})$. We explicitly include the dependence of the Ca^{2+} concentration on n_{10}. The reason is that the number of activable subunits determines the number of open channels n_c and hence c. However, the mere value of n_{10} does not uniquely fix n_c. It is the distribution of the n_{10} subunits on the N receptors that defines n_c. This follows from the minimal number of activated subunits for channel opening. For example 9 activable subunits in a group of 6 IP_3Rs can lead to 3 open or 6 closed channels because a channel may open when at least 3 subunits are in the state 10. It turns out that the distribution of n_c for a given value of n_{10} is sharply peaked. This is explained in detail in appendix A.1. Hence we will use the mean of that distribution to compute the number of open channels from n_{10}.

Having fixed n_c we now relate it to the Ca^{2+} concentration. The basic idea is to conceive a cluster as a tightly packed array of a small number of channels. Several aspects of it have already been mentioned in section 3.4. We will demonstrate here how this deterministic description is motivated by the stochastic dynamics of N IP_3Rs . Consider $n_c \leq N$ channels in the open state. Then Ca^{2+} flows from the ER to the cytosol through a fraction n_c/N of the whole cluster area. As the spatial arrangement of the IP_3 channels does not influence the dynamics of the concentration (Swillens et al. 1999), the flux is uniquely determined by the ratio n_c/N. In the case of a spherical cluster - merely for simplifying the calculation we assume it to be a sphere rather than a membrane patch - we map the n_c open channels to a concentrical sphere that occupies the (n_c/N)th part of the whole sphere, i.e the total cluster. Hence any number of open channels $0 \leq n_c \leq N$ corresponds to a concentrical region whose volume is given by a fraction n_c/N of the maximal value. Identifying a given n_c with the radius a of the corresponding sphere we arrive at

$$a = a_0 \sqrt[3]{\frac{n_c}{N}} = a_0 \frac{I}{I+d_1} \sqrt[3]{\frac{n_{10}}{3N} \frac{n_{10}-1}{3N-1} \frac{n_{10}-2}{3N-2}}\,, \tag{4.2}$$

where we inserted equation (A.14) for n_c. Equation (4.2) naturally incorporates the lower and upper bound of a cluster. If $n_c = 0$, then $a = 0$ and no Ca^{2+} is liberated from the ER. On the other hand if all channels are open, a takes its maximal value a_0. In the limit $n_{10} \to \infty, N \to \infty$ we recover equation (3.26) if we apply equation (A.15) in equation (4.2). In this respect the above discussion justifies a posteriori the approach we have chosen in chapter 2. On the basis of a discrete number of IP_3Rs, we realize that the radius of the source area is directly determined by the number of open channels. There is no need

for solving an implicit equation. It only arises in the continuous limit. Therefore taking the small number of receptors per cluster seriously provides us with an intuitive picture of the cluster dynamics. For further calculations we simplify equation (4.2) due to $3N \gg 1$, so that the final form is

$$a = a_0 \frac{I}{I + d_1} \sqrt[3]{\frac{n_{10}}{3N} \frac{n_{10} - 1}{3N} \frac{n_{10} - 2}{3N}} \,. \tag{4.3}$$

Equipped with equation (4.3) we return to the Ca^{2+} profiles of section . 3.4. The formalism developed there remains valid, although a is not a smoothly varying function any more. The general notion foots on calculating the Ca^{2+} profiles for each n_{10}. Then the radius $a = a(n_{10})$ is constant in these computations. The time evolution of a cluster for which the radius takes on only discrete values can be imagined as follows. Suppose that at time t the radius changes from a value a_1 to a value a_2. Although this is a discontinuous step in the radius the Ca^{2+} concentration is to change continuously in time for every spatial coordinate. Therefore we set the initial conditions for the profile with $a = a_2$ such that they correspond to the final values for the profile with $a = a_1$. The above procedure allows us to use time dependent Ca^{2+} profiles in equation (4.1). However, the results of chapter 1 indicate that employing stationary solutions is a reasonable approximation. The flux simulations have shown that the Ca^{2+} concentration at a single channel responds within microseconds upon opening and closing, whereas typical dwell times are in the range of a few milliseconds. Hence, the Ca^{2+} concentration at a cluster almost immediately follows a change in the number of open channels and then stays constant. Neglecting that fast initial transient, we express the Ca^{2+} concentration in equation (4.1) by the fixed point solution (3.26) . It is uniquely determined by the value of $a = a(n_{10})$, so that equation (4.1) is eventually closed.

4.3 Fokker-Planck equations

Although master equations represent the most accurate description of microscopic dynamics, only a few exact solutions exist at the moment. Especially nonlinear equations like (4.1) often resist to a direct treatment. In this case several approximations have been put forward (Van Kampen 2001, Moyal 1949, Kramers 1940, Grabert et al. 1983, Hänggi et al. 1984). Despite the plethora of methods there still is no consensus which approximation is the best (Gitterman and Weiss 1991). Each of them possesses advantages and drawbacks, so that the problem at hand finally decides which procedure to use. In this section we will apply the Fokker-Planck equations to estimate the mean first passage time in a bistable potential,

see section 4.4. Hence, the results depend on the way the different Fokker-Planck equations treat the fluctuations because noise drives the escape process. We will concentrate on van Kampen's Ω expansion and a method that is similar to that of a Kramers-Moyal expansion. Whereas the latter keeps the nonlinearities of the master equation in the fluctuations, the former approximates them in a linear fashion. Therefore, they represent antipodes in treating the noise which is the reason for studying both of them.

The Ω expansion is based on the observation that a fluctuating quantity n can be characterized by a macroscopic variable ϕ and the fluctuations ξ. This leads to the ansatz $n = \Omega\phi + \Omega^{1/2}\xi$. Thinking of Ω as the volume of a system, it corresponds to relating an intensive variable ϕ to an extensive variable n with some noise ξ. Moreover, we see that the fluctuations are of order $\Omega^{-1/2}$ with respect to the intensive variable as is to be expected. Note that the volume is not a necessary interpretation of Ω. It suffices that some small parameter exists in the master equation that can be identified with Ω^{-1}.

For the master equation (4.1) the number of subunits hN will serve as the expansion parameter. On the one hand $hN \gg 1$ for a realistic cluster of IP_3 receptors, on the other hand the limit $hN \to \infty$ produces the macroscopic equations. This is in agreement with the above ansatz for n, because in the deterministic limit fluctuations vanish and the system is correctly described by ϕ alone. For the two dimensional master equation, the preceding discussion leads to the definitions

$$n_{10} = \Omega\phi(t) + \Omega^{\frac{1}{2}}\xi\,, \quad n_{\bar{h}} = \Omega\psi(t) + \Omega^{\frac{1}{2}}\eta\,, \tag{4.4a}$$

$$P(n_{10}, n_{\bar{h}}, t) = \Pi(\xi, \eta, t)\,. \tag{4.4b}$$

Equations (4.4a) can be understood as transformations of the variables n_{10} and $n_{\bar{h}}$ to the new variables ξ and η with still unknown time dependent functions $\phi(t)$ and $\psi(t)$. The goal of van Kampen's Ω expansion is to derive equations for $\phi(t)$ and $\psi(t)$ as well as for the new probability $\Pi(\xi, \eta, t)$. To this aim we start with the left hand side of the master equation. Using equations (4.4) we find

$$\frac{\partial \Pi}{\partial t} = \frac{\partial P}{\partial t} + \frac{\partial P}{\partial n_{10}}\frac{\partial n_{10}}{\partial t} + \frac{\partial P}{\partial n_{\bar{h}}}\frac{\partial n_{\bar{h}}}{\partial t} = \frac{\partial P}{\partial t} + \Omega^{\frac{1}{2}}\frac{\partial \Pi}{\partial \xi}\frac{\partial \phi}{\partial t} + \Omega^{\frac{1}{2}}\frac{\partial \Pi}{\partial \eta}\frac{\partial \psi}{\partial t}\,. \tag{4.5}$$

The right hand side requires more considerations. For the probability P a term

like $P(n_{10} \pm 1, n_{\bar{h}})$ is transformed to the new variables according to

$$\begin{aligned} P(n_{10} \pm 1, n_{\bar{h}}) =& P(\Omega\phi(t) + \Omega^{\frac{1}{2}}\xi \pm 1, \Omega\psi(t) + \Omega^{\frac{1}{2}}\eta) \\ =& P(\Omega\phi(t) + \Omega^{\frac{1}{2}}(\xi \pm \Omega^{-\frac{1}{2}}), \Omega\psi(t) + \Omega^{\frac{1}{2}}\eta) \\ =& \Pi(\xi \pm \Omega^{-\frac{1}{2}}, \eta) \\ =& \Pi(\xi, \eta) \pm \Omega^{-\frac{1}{2}}\frac{\partial \Pi}{\partial \xi} + \frac{1}{2}\Omega^{-1}\frac{\partial^2 \Pi}{\partial \xi^2} + \mathcal{O}(\Omega^{-\frac{3}{2}}) \end{aligned} \tag{4.6}$$

All other expressions of P are handled analogously. For the transition rates w we firstly show that they obey the usual scaling $w(n_{10}, n_{\bar{h}}) = \Omega\tilde{w}(n_{10}/\Omega, n_{\bar{h}}/\Omega)$. Expanding (4.3) results in

$$a = a_I \sqrt[3]{\left(\frac{n_{10}}{\Omega}\right)^3 - \frac{1}{N}\left(\frac{n_{10}}{\Omega}\right)^2 + \frac{2}{\Omega}\left(\frac{n_{10}}{\Omega}\right)} = \frac{a_I n_{10}}{\Omega} - \frac{a_I}{\Omega} + \mathcal{O}(\Omega^{-2}) \tag{4.7}$$

with $a_I := a_0 I/(I + d_1)$. Hence, the Ca^{2+} concentration reads

$$c(n_{10}) = \tilde{c}\left(\frac{a_I n_{10}}{\Omega}\right) - \frac{d\tilde{c}}{da}\left(\frac{a_I n_{10}}{\Omega}\right)\frac{a_I}{\Omega} + \mathcal{O}(\Omega^{-2})\,. \tag{4.8}$$

This establishes the above scaling because all rates posses the form $w(n_{10}, n_{\bar{h}}) = g(n_{10}, n_{\bar{h}})f(c(n_{10}))$ with a linear function g and some function f. For instance consider the expression $[hN - n_{10} - n_{\bar{h}}]a_5 c(n_{10})$. Then

$$g(n_{10}, n_{\bar{h}}) = hN - n_{10} - n_{\bar{h}} = \Omega\left[1 - \frac{n_{10}}{\Omega} - \frac{n_{\bar{h}}}{\Omega}\right], \tag{4.9a}$$

$$f(c(n_{10})) = a_5 c(n_{10}) = a_5\left[\tilde{c}\left(\frac{a_I n_{10}}{\Omega}\right) - \frac{d\tilde{c}}{da}\left(\frac{a_I n_{10}}{\Omega}\right)\frac{a_I}{\Omega} + \mathcal{O}(\Omega^{-2})\right]. \tag{4.9b}$$

Note that the term $c(n_{10})$ only emphasizes the dependence of the Ca^{2+} concentration on n_{10}, but that the function $\tilde{c}$ denotes the Ca^{2+} profiles of section 3.4. In the remainder we will drop the swung dash to ease the notation. The specific scaling of the rates allows an expansion in analogy to equation (4.6). Employing the rate $w(n_{10}+1, n_{\bar{h}})$ as an representative example, we find with $(x, y) \mapsto \tilde{w}(x, y)$ up to second order

$$\begin{aligned} w &= \Omega\tilde{w}\left(\phi + \Omega^{-\frac{1}{2}}(\xi + \Omega^{-\frac{1}{2}}), \psi + \Omega^{-\frac{1}{2}}\eta\right) \\ &= \Omega\tilde{w}\left(\phi + \Omega^{-\frac{1}{2}}\xi, \psi + \Omega^{-\frac{1}{2}}\eta\right) + \Omega^{\frac{1}{2}}\frac{\partial \tilde{w}}{\partial \xi}\left(\phi + \Omega^{-\frac{1}{2}}\xi, \psi + \Omega^{-\frac{1}{2}}\eta\right)\Big|_\xi \\ &= \Omega\tilde{w}\,(\phi, \psi) + \Omega^{\frac{1}{2}}\left(\frac{\tilde{w}}{\partial x}\Big|_{\phi,\psi}\xi + \frac{\tilde{w}}{\partial y}\Big|_{\phi,\psi}\eta\right) + \frac{\partial}{\partial \xi}\left(\frac{\tilde{w}}{\partial x}\Big|_{\phi,\psi}\xi + \frac{\tilde{w}}{\partial y}\Big|_{\phi,\psi}\eta\right)\Big|_\xi \end{aligned} \tag{4.10}$$

Equations like (4.6) and (4.10) serve as the building blocks for the Ω expansion. Rewriting all the terms of the master equation (4.1) in the new variables, we find that the lowest non vanishing order is $\mathcal{O}(\Omega^{\frac{1}{2}})$. It leads to the equation

$$\frac{\partial \Pi}{\partial \xi}\frac{\partial \phi}{\partial t} + \frac{\partial \Pi}{\partial \eta}\frac{\partial \psi}{\partial t} = \frac{\partial \Pi}{\partial \xi} f_1 + \frac{\partial \Pi}{\partial \eta} f_2 \,, \tag{4.11}$$

with

$$f_1 := -\phi(a_5 c + a_6 c + b_5) + \psi\left(\frac{b_6 c}{c + d_5} - a_5 c\right) + a_5 c \,, \tag{4.12a}$$

$$f_2 := -(a_6 c + b_6)\psi + a_6 c \,. \tag{4.12b}$$

and $c := c(a_I \phi)$. It is a necessary condition for the validity of the Ω expansion that equation (4.11) is always fulfilled. Otherwise, the expansion would include terms that diverge in the limit $\Omega \to \infty$ and therefore would not be mathematically sound. Fortunately, equation (4.11) always holds due to

$$\frac{\partial \phi}{\partial t} = f_1 \,, \qquad \frac{\partial \psi}{\partial t} = f_2 \,. \tag{4.13}$$

They constitute the macroscopic equations of the underlying microscopic process, see equation (3.20). The solutions of (4.13) represent the time dependent transformations in equation (4.4). They tend to the fixed points

$$\bar{\phi} = \frac{d_6 c}{(c + d_5)(c + d_6)} \,, \qquad \bar{\psi} = \frac{c}{c + d_6} \,, \tag{4.14}$$

which are in agreement with the results of section 3.3. Note that $\bar{\phi}$ is computed from an implicit equation due to $c = c(a_I \bar{\phi})$. This may result in multiple fixed points as depicted in figure 4.1. It shows the nullclines of the macroscopic equations.

For the parameters chosen we find a region of bistability as in the previous chapter. Increasing the IP_3 concentration shifts the curve for $\dot{\phi} = 0$ upwards. It gives rise to a saddle node bifurcation. The second saddle node bifurcation occurs when lowering I. Hence figure 4.1 is equivalent to figure 3.5.

Proceeding to the next order $\mathcal{O}(1)$ in the Ω expansion we find

$$\begin{aligned} \frac{\partial \Pi}{\partial t} =& -\left[g_{11}\frac{\partial}{\partial \xi} + g_{21}\frac{\partial}{\partial \eta}\right](\xi \Pi) - \left[g_{12}\frac{\partial}{\partial \xi} + g_{22}\frac{\partial}{\partial \eta}\right](\eta \Pi) \\ &+ \frac{1}{2}\left(h_{11}\frac{\partial^2}{\partial \xi^2} + 2h_{12}\frac{\partial^2}{\partial \eta \partial \xi} + h_{22}\frac{\partial^2}{\partial \eta^2}\right)\Pi \,. \end{aligned} \tag{4.15}$$

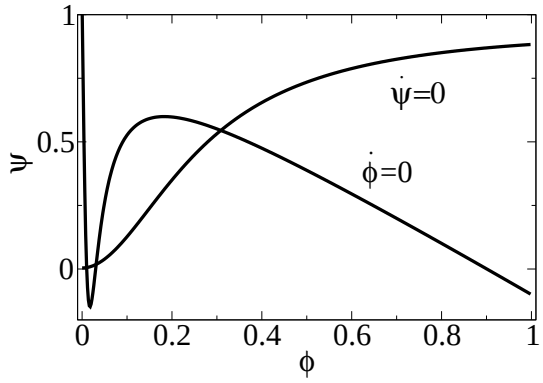

Figure 4.1: Nullclines of equation (4.13) for $d_1 = 0.13\mu M, d_2 = 12.588\mu M, d_3 = 0.9434\mu M, d_4 = 1.73462\mu M, d_5 = 2.4702\mu M, k_p = 80s^{-1}, k_l = 0.002s^{-1}, k_c = 700s^{-1}, E = 750\mu M, a_0 = 0.11\mu m, D = 40\mu m^2 s^{-1}, I = 0.3\mu M$.

The matrices (g_{ij}) and (h_{ij}) with $h_{12} = h_{21}$ are defined as

$$g_{11} := b_6 d_5 \psi c^1/(c+d_5)^2 - a_6\,(c+\phi c) - b_5 - a_5\left(c-(1-\phi-\psi)c^1\right)\,, \tag{4.16a}$$

$$g_{21} := a_6 c^1 - a_6 \psi c^1\,, \tag{4.16b}$$

$$g_{12} := b_6 c/(c+d_5) - a_5 c\,, \tag{4.16c}$$

$$g_{22} := -\left(a_6 c + b_6\right)\,, \tag{4.16d}$$

and

$$h_{11} := a_5(1-\psi-\phi)c + b_6\psi c/(c+d_5) + a_6\phi c\,, \tag{4.17a}$$

$$h_{21} := b_6\psi c/(c+d_5) + a_6\phi c\,, \tag{4.17b}$$

$$h_{22} := a_6(1-\psi-\phi)c + b_6\psi c/(c+d_5) + a_6\phi c\,. \tag{4.17c}$$

with $c^1 := dc/da(a_I\phi)a_I$. For the symmetric matrix (h_{ij}) the Hurwitz criterion assures that it is positive semi-definite. This ensues that equation (4.15) represents a linear multivariate Fokker-Planck equation. From a technical point of view, this is clearly an advantage of the Ω expansion, because linear Fokker-Planck equations can be solved analytically. If $-\infty < \xi, \eta < \infty$ a solution of equation (4.15) is a Gaussian. Therefore it suffices to calculate the two first moments. The averages are governed by the equations

$$\partial_t \langle\xi\rangle = g_{11}\langle\xi\rangle + g_{12}\langle\eta\rangle\,, \tag{4.18a}$$

$$\partial_t \langle\eta\rangle = g_{21}\langle\xi\rangle + g_{22}\langle\eta\rangle\,. \tag{4.18b}$$

They are the same as the variational equations associated with the macroscopic laws. This can be seen by linearizing equation (4.13) and substituting the linear perturbations with the corresponding averages. The three second moments obey the equations

$$\partial_t \left\langle \xi^2 \right\rangle = 2g_{11} \left\langle \xi^2 \right\rangle + 2g_{12} \left\langle \xi\eta \right\rangle + h_{11} \,, \tag{4.19a}$$

$$\partial_t \left\langle \eta^2 \right\rangle = 2g_{21} \left\langle \xi\eta \right\rangle + 2g_{22} \left\langle \eta^2 \right\rangle + h_{22} \,, \tag{4.19b}$$

$$\partial_t \left\langle \xi\eta \right\rangle = g_{11} \left\langle \xi\eta \right\rangle + g_{12} \left\langle \eta^2 \right\rangle + g_{21} \left\langle \xi^2 \right\rangle + g_{22} \left\langle \eta\xi \right\rangle + h_{21} \,. \tag{4.19c}$$

For a finite range of ξ and η the solution of equation (4.15) cannot be expressed as a Gaussian anymore. We provide a corresponding example in section 4.4.1. However, the Ω expansion is mostly applied to unrestricted noise so that solving equations 4.18 and 4.19 is usually enough.

The linear character of the noise has cast some doubts about the validity of the Ω expansion in the past. It has been criticized that in nonlinear systems a linear description as equation (4.15) would not capture the correct nature of the fluctuations. To estimate the differences between a linear and a nonlinear delineation of the noise we now derive a nonlinear Fokker-Planck equation for the probability P.

The basic concept of this approximation is that we can deal with the shifts $n_{10} \pm 1, n_{\bar{h}} \pm 1$ of n_{10} and $n_{\bar{h}}$ in equation (4.1) by means of a Taylor expansion. This yields up to second order

$$\begin{aligned}
\frac{\partial P}{\partial t} =& \frac{\partial}{\partial n_{10}} \left[n_{10} a_6 c(n_{10}) + n_{10} b_5 - (hN - n_{\bar{h}} - n_{10}) a_5 c(n_{10}) \right] P \\
&- \frac{\partial}{\partial n_{10}} \left[\frac{b_6 c(n_{10})}{c(n_{10}) + d_5} n_{\bar{h}} \right] P + \frac{\partial}{\partial n_{\bar{h}}} \Big[b_6 - (Nh - n_{\bar{h}}) a_6 c(n_{10}) \Big] P \\
&+ \frac{\partial^2}{2\partial n_{10}^2} \left[n_{10} a_6 c(n_{10}) + n_{10} b_5 + (hN - n_{\bar{h}} - n_{10}) a_5 c(n_{10}) \right] P \\
&+ \frac{\partial^2}{2\partial n_{10}^2} \left[\frac{b_6 c(n_{10})}{c(n_{10}) + d_5} n_{\bar{h}} \right] P + \frac{\partial^2}{2\partial n_{\bar{h}}^2} \Big[b_6 + (Nh - n_{\bar{h}}) a_6 c(n_{10}) \Big] P \\
&- \frac{\partial}{\partial n_{\bar{h}} \partial n_{10}} \left[n_{10} a_6 c(n_{10}) + \frac{b_6 c(n_{10})}{c(n_{10}) + d_5} \right] P \,.
\end{aligned} \tag{4.20}$$

The scaling of the transition rates (ref. equation (4.7)) motivates the introduction of new variables $\phi := n_{10}/\Omega$ and $\psi := n_{\bar{h}}/\Omega$ with $\Omega = hN$. Note that they are

different from those for the Ω expansion. Then, the new probability $p(\phi, \psi, t) := P(n_{10}/\Omega, n_{\bar{h}}/\Omega)$ is governed by

$$\begin{aligned}\frac{\partial p}{\partial t} =& \frac{\partial}{\partial \phi}\left[\phi a_6 c + \phi b_5 - (1-\psi-\phi)a_5 c - \frac{b_6 c}{c+d_5}\psi\right] p \\ &+ \frac{\partial^2}{2\Omega \partial \phi^2}\left[\phi a_6 c + \phi b_5 + (1-\psi-\phi)a_5 c + \frac{b_6 c}{c+d_5}\psi\right] p \\ &+ \frac{\partial}{\partial \psi}\Big[b_6 - (1-\psi)a_6 c\Big] p + \frac{\partial^2}{2\Omega \partial \psi^2}\Big[b_6 + (1-\psi)a_6 c\Big] p \\ &- \frac{\partial}{\Omega \partial \psi \partial \phi}\left[\phi a_6 c + \frac{b_6 c}{c+d_5}\right] p\,.\end{aligned} \tag{4.21}$$

with the former notation $c = c(a_I \phi)$. A comparison of equation (4.21) to equations (4.13) and (4.15) elucidates the formal differences between the two approaches. Whereas the first keeps all the nonlinearities of the original master equation, the second only includes them in the macroscopic equation. Such a difference is the more striking as both approximations stem from the same master equation. However, this result may be attributed to the assumptions they are based upon. Whereas van Kampen's approach is guided by the picture of a macroscopic variable whose state space is diffusively broadened by the noise, equation (4.21) only supposes that the jumps between adjacent configurations are small. To decide from scratch which of the two Fokker-Planck equations approximates the master equation best, is a difficult task and essentially depends on the question under investigation (Gitterman and Weiss 1991). In the subsequent section we will apply both methods to compute the mean first passage time for a bistable system. It is a quantity that only exists in noisy systems and demonstrates the role of fluctuations.

4.4 Waiting time distribution

4.4.1 General framework

A deterministic system which has reached equilibrium never leaves this state. However, as soon as fluctuations have to be taken into account, the life time in this state may become finite. That holds in particular in the bistable regime. A system that shows such a dynamical behavior can be described by a double well potential U as depicted in figure 4.2. Here the states A and C are stable, whereas B is unstable. This means that the system spends most of the time in A or C. It

can leave one of these stable states by fluctuations carrying it across the barrier B and eventually reaches the other state. The frequency of these transitions depend on the shape of the potential. In figure 4.2 it is easier to go from A to C than in the opposite direction. Firstly, the potential difference between A and B is much lower than between C and B, and secondly the states A and B are closer together in the x direction than C and B.

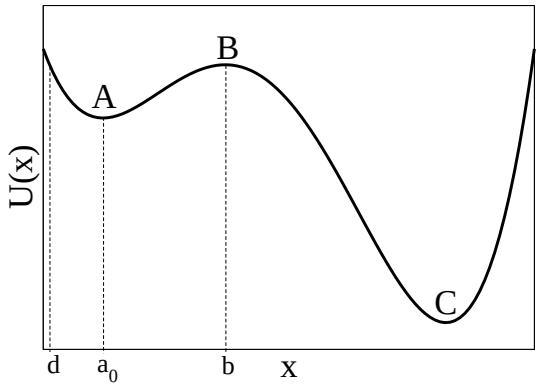

Figure 4.2: Bistable potential $U(x)$. The states A and C are stable whereas B is unstable.

In the remainder of the section we will concentrate on the escape from state A. This corresponds to the process when a system prepared in state A reaches state B for the first time. The time that the reaching of B takes is a stochastic variable because the motion is governed by the fluctuations. Therefore, we compute the probability density $\rho(a_0, t)$ that a system which starts out at $x = a_0$ at $t = 0$ reaches $x = b$ for the first time in the interval t and $t + dt$.

The calculation of ρ requires a more precise formulation of the escape process. The notion of counting a system's arrival at B only for the first time means that it must not leave b once it has got there. Otherwise, it would possess the opportunity to reach B for more than one time. Mathematically, such a condition is implemented by an absorbing boundary at b. Hence, b represents the upper bound for the system's dynamics. It remains the question for the lower bound. Here, we set d to some finite value. Such a lower bound occurs frequently for stochastic variables. For instance, the number of particles should always be positive, or the price of a share should not drop below a lower limit. In contrast to the upper bound, we establish a reflecting boundary condition at $x = d$. Thus, as soon as the system reaches d, it proceeds to states $x > d$. This is motivated by the behavior of the master equation. When the systems reaches the state $(n_{10}, n_{\bar{h}}) = (0, 0)$ it can only evolve toward positive values of $(n_{10}, n_{\bar{h}})$. For our

further analysis, we will refer to the interval $[d, b]$ as the left well of the bistable potential.

The density ρ may be obtained from a master equation as well as from a Fokker-Planck equation. For the latter it is convenient to introduce a new quantity $G(a_0, t)$. It represents for the probability that a system is still inside the left well at time t when it has been prepared at $x = a_0$ at $t = 0$. Let $\mathcal{L}$ denote the Fokker-Planck operator, then the time evolution of G is governed by the adjoint operator $\tilde{\mathcal{L}}$. Up to now no general solution has been worked out for an arbitrary $\mathcal{L}$. Yet, an analytic expression for G is available for a linear Fokker-Planck operator. It is given by the solution of (Gardiner 1985)

$$\frac{\partial G(x,t)}{\partial t} = -vx\frac{\partial G(x,t)}{\partial x} + \frac{w}{2}\frac{\partial^2 G(x,t)}{\partial x^2}\,, \qquad v, w > 0\,, \tag{4.22}$$

where v, w are arbitrary constants. The initial and boundary conditions for equation (4.22) are

$$G(x,0) = \begin{cases} 1, & d \le x \le b \\ 0, & else \end{cases}\,, \quad \frac{\partial G(d,t)}{\partial x} = 0 \quad \forall t\,, \quad G(b,t) = 0 \quad \forall t\,. \tag{4.23}$$

The initial condition states that at $t = 0$ the system is still in the left well with probability one. The reflecting boundary condition at $x = d$ is expressed by a no-flux boundary condition. This is equal to a vanishing derivative at $x = d$ because we investigate the adjoint Fokker-Planck equation. Setting $G \equiv 0$ at the right boundary corresponds to instantly removing the system from the well as soon as it reaches b. This is the descriptive meaning of an absorbing boundary. We solve equation (4.22) with the ansatz $G(x,t) = \exp(-\lambda t)u(x), \lambda \ge 0$ so that it reduces to the ordinary differential equation

$$\frac{d^2u}{dx^2} - \frac{2vx}{w}\frac{du}{dx} + \frac{2\lambda}{w}u = 0\,. \tag{4.24}$$

Applying the transformation $z := x^2/4$ we find for $\bar{u}(z) := u(x)$

$$z\frac{d^2\bar{u}}{dz^2} + \left(\frac{1}{2} - \frac{4vz}{w}\right)\frac{d\bar{u}}{dz} + \frac{2\lambda}{w}\bar{u} = 0\,. \tag{4.25}$$

It equals Kummer's equation for $\tilde{u}(\tilde{z}) := \bar{u}(z)$ by setting $\tilde{z} := 4vz/w$

$$\tilde{z}\frac{d^2\tilde{u}}{d\tilde{z}^2} + \left(\frac{1}{2} - \tilde{z}\right)\frac{d\tilde{u}}{d\tilde{z}} + \frac{\lambda}{2v}\tilde{u} = 0\,. \tag{4.26}$$

Hence two independent solutions of equation (4.24) read (Abramowitz and Stegun 1974)

$$u_1(x) := M\left(-\frac{\lambda}{2v}, \frac{1}{2}, \frac{vx^2}{w}\right)\,, \quad u_2(x) := xM\left(\frac{1}{2} - \frac{\lambda}{2v}, \frac{3}{2}, \frac{vx^2}{w}\right)\,. \tag{4.27}$$

M designates the confluent hypergeometric function

$$M(p,q,x) := \sum_{k=0}^{\infty} \frac{(p)_k}{(q)_k} \frac{x^k}{k!}\,, \tag{4.28}$$

where $(p)_0 := 1$ and $(p)_k := p(p+1)\ldots(p+k-1)$. The boundary condition at $x = b$ entails that a solution of equation (4.24) is

$$u(x) := C_1 \left[u_1(x) - \frac{u_1(b)}{u_2(b)} u_2(x) \right] = u_1(x) - \frac{u_1(b)}{u_2(b)} u_2(x)\,. \tag{4.29}$$

Without loss of generality we set $C_1 = 1$ as it merely serves as normalization. The second boundary condition fixes the still unknown eigenvalues λ. They constitute an infinite countable set $\{\lambda_n\}$ due to the finiteness of a and b. Therefore the general solution of equation (4.22) can be expressed as

$$G(x,t) = \sum_{n=0}^{\infty} a_n \exp(-\lambda_n t) u_n(x)\,. \tag{4.30}$$

The subscript of $u_n(x)$ indicates that equation (4.29) has to be evaluated at $\lambda = \lambda_n$. The coefficients a_n are determined by the initial condition $g(x,0)$ which results in

$$a_n = \int_d^b r(x) u_n(x) dx \Bigg/ \int_d^b r(x) u_n^2(x) dx\,, \quad r(x) := \frac{2}{w} \exp\left(-\frac{v}{w} x^2\right). \tag{4.31}$$

Here we used the orthogonality relation of the eigenfunctions $u_n(x)$:

$$\int_d^b u_n(x) u_m(x) r(x) dx = \delta_{m,n} \int_d^b u_n^2(x) r(x) dx\,. \tag{4.32}$$

The probability $\rho(x,t)$ that a particle leaves the well between t and $t + dt$ is readily computed from $G(x,t)$ as $\rho = -\partial_t G(x,t)$. Hence the mean first passage time $T(x)$ equals

$$T(x) := \langle t(x) \rangle = \int_0^{\infty} t \rho(x,t) dt = -\int_0^{\infty} t \partial_t G(x,t) dt\,. \tag{4.33}$$

Note that ρ is already normalized to 1 due to the initial condition $G(x,0)$.

An alternative approach to the mean first passage time follows from the differential equation (Gardiner 1985)

$$-vx \frac{dT(x)}{dx} + \frac{w}{2} \frac{d^2 T(x)}{dx^2} = -1\,, \tag{4.34}$$

with the solution

$$T(x) = \frac{2}{w}\int_x^b \frac{dy}{h(y)}\int_d^y h(z)dz\,, \quad h(x) := \exp\left\{-\frac{v}{w}(x^2-d^2)\right\}\,. \tag{4.35}$$

Performing the z integration we find

$$\begin{aligned} T(x) =& \sqrt{\frac{\pi}{vw}}\int_x^b dy \exp\left(-\frac{v}{w}y^2\right)\operatorname{erf}\left(\sqrt{\frac{v}{w}}y\right) \\ &+ \frac{\pi}{2v}\operatorname{erf}\left(\sqrt{\frac{v}{w}}d\right)\left\{\operatorname{erfi}\left(\sqrt{\frac{v}{w}}x\right) - \operatorname{erfi}\left(\sqrt{\frac{v}{w}}b\right)\right\}\,. \end{aligned} \tag{4.36}$$

The functions $\operatorname{erf}(x)$ and $\operatorname{erfi}(x) = \operatorname{erf}(ix)/i$ stand for for the Gaussian error function and the imaginary Gaussian error function, respectively. The remaining integral can be solved by series expansion so that the final expression for the mean first passage takes the form

$$\begin{aligned} T(x) =& \frac{b^2}{w}F_{2;2}\left(1,1;\frac{3}{2},2;\frac{w}{v}b^2\right) - \frac{x^2}{w}F_{2;2}\left(1,1;\frac{3}{2},2;\frac{w}{v}x^2\right) \\ &+ \frac{\pi}{2v}\operatorname{erf}\left(\sqrt{\frac{v}{w}}d\right)\left\{\operatorname{erfi}\left(\sqrt{\frac{v}{w}}x\right) - \operatorname{erfi}\left(\sqrt{\frac{v}{w}}b\right)\right\}\,. \end{aligned} \tag{4.37}$$

We employed the generalized hypergeometric function

$$F_{p;q}(a_1,\ldots,a_p;b_1,\ldots,b_q;x) = \sum_{l=0}^{\infty}\frac{(a_1)_l\cdots(a_p)_l}{(b_1)_l\cdots(b_q)_l}\frac{x^l}{l!}\,, \tag{4.38}$$

and used the identiy

$$\frac{j!}{2j+2}\sum_{l=0}^{j}\frac{(-1)^l}{(2l+1)(j-l)!l!} = \frac{1}{2}\frac{(1)_j(1)_j}{\left(\frac{3}{2}\right)_j(2)_j}\,. \tag{4.39}$$

We defer the proof of it to the appendix A.2. The reason for presenting two methods for evaluating the mean first passage time is based on their different scopes of applicability. If we were only interested in T, then equation (4.37) would be preferable because it requires less computation. However, we are limited to the first moment. Differential equations for higher moments couple to the lower ones leading to a system of ODEs (Gardiner 1985). This is the advantage of the first approach. We obtain any moment by one integration. Moreover, we have access to the time evolution of the escape process which allows for a more detailed analysis.

The above results could only be obtained analytically because the corresponding Fokker-Planck equation was linear. In the case of a nonlinear Fokker-Planck equation, all quantities have to be computed numerically. The mean first passage time is evaluated best from a generalization of equation (4.35). For $\mathcal{L} = \partial_x A(x) + \partial_x^2 B(x)/2$ we find (Gardiner 1985)

$$T(x) = 2 \int_x^b \frac{dy}{h(y)} \int_a^y \frac{h(z)}{B(z)} dz \,, \quad h(x) := \exp\Big\{ \int_a^x \frac{2A(y)}{B(y)} dy \Big\} \,. \tag{4.40}$$

The study of Fokker-Planck equations instead of master equations is often motivated by the easier treatment of the former. It holds in particular in higher dimensions, because a broader spectrum of tools is available for Fokker-Planck equations than for master equations (Risken 1984). This constitutes one of the reasons for the derivations in section 4.3. However, Fokker-Planck equations always represent approximations. The only way to test their quality is a comparison with results obtained from a master equation. In general they stem from numerical integrations. Yet, the mean first passage time can be computed analytically in one dimension.

We consider a one step process that starts at a site m at $t = 0$. Being at site n the particle hops to the right with a rate g_n and to the left with a rate r_n, respectively. When it reaches the left boundary L, it is reflected. Then, the mean first passage time to arrive at a site $R > m$ reads (Van Kampen 2001)

$$T_{R,m} = \sum_{i=m}^{R-1} \left(\frac{1}{g_i} + \sum_{l=L+1}^{i} \frac{r_i r_{i-1} \cdots r_l}{g_i g_{i-1} \cdots g_l} \frac{1}{g_{l-1}} \right) \,. \tag{4.41}$$

This allows us to estimate the validity of the preceding approximations. Although escape problems in higher dimensions behave differently than in one dimension - a system possesses additional paths out of a stable fixed point - the above discussion provides a starting point for reasonably choosing a Fokker-Planck equation in higher dimensions.

4.4.2 Ca^{2+} dynamics

We now apply the results of section 4.4.1 to the dynamics of an IP_3R cluster. The behavior that is most frequently found for a single cluster is a Ca^{2+} puff. It is the concerted opening of approximately five channels (Sun et al. 1998). The small number of channels per cluster induces large fluctuations in the number of open channels. A possible mechanism how this noise leads to a puff can be

conceived as follows. Suppose that the state of a cluster after recovery from inhibition resembles state A of figure 4.2. Whenever the fluctuations carry it over the barrier a new puff starts. Thus we may estimate the stochastic fraction of the puff period from the mean first passage time for a process as described in the previous section. Note that the mean first passage time is always smaller than the puff period measured in experiments.

The master equation (4.1) describes the stochastic dynamics of one IP_3R cluster. It yields the probability for a configuration $(n_{10}, n_{\bar{h}})$ of activable and inhibited subunits. They determine the number of open channels. Consequently, all information for the initiation of a puff is included in the master equation. However, no general solution for a two dimensional escape problem has been found by now. Only a few results exist. See (Henry and Levine 2003) for a recent contribution. Therefore we approximate equation (4.1) by a one dimensional expression. It allows to use all methods presented in the section 4.4.1.

The reduction of equation (4.1) to one dimension is achieved by keeping $n_{\bar{h}}$ constant. The reason lies in the different time scales for the dynamics of n_{10} and $n_{\bar{h}}$. The latter is controlled by Ca^{2+} inhibition which is much slower than Ca^{2+} activation. When n_{10} changes, the value of $n_{\bar{h}}$ remains almost constant. This leads to the one dimensional master equation

$$\begin{aligned}\dot{P}(n_{10}) = &- \frac{b_6 c(n_{10})}{c(n_{10}) + d_5} n_{\bar{h}} P(n_{10}) + \frac{b_6 c(n_{10}-1)}{c(n_{10}-1) + d_5} n_{\bar{h}} P(n_{10}-1) \\ &- (hN - n_{10} - n_{\bar{h}}) a_5 c(n_{10}) P(n_{10}) + b_5 (n_{10}+1) P(n_{10}+1) \\ &- b_5 n_{10} P(n_{10}) + (hN - n_{10} - n_{\bar{h}} + 1) a_5 c(n_{10}-1) P(n_{10}-1) \\ &- a_6 c(n_{10}) n_{10} P(n_{10}) + a_6 (n_{10}+1) c(n_{10}+1) P(n_{10}+1)\,.\end{aligned} \tag{4.42}$$

The Fokker-Planck equations for equation (4.42) that correspond to equations (4.15) and (4.21) can be directly deduced from them. It suffices to set all derivatives with respect to η and $n_{\bar{h}}$ equal to zero, respectively. This holds because of $n_{\bar{h}} = const.$ It results in a linear Fokker-Planck equation for ξ with the same sign convention as equation (4.22) due to $g_{11} < 0$ and $h_{11} > 0$. For full compliance with section 4.4.1, we have to consider the macroscopic equation. It follows from equation (4.13) as

$$\dot{\phi} = -\phi(a_5 c + a_6 c + b_5) + \bar{\psi}\left(\frac{b_6 c}{c + d_5} - a_5 c\right) + a_5 c\,, \tag{4.43}$$

with the constant $\bar{\psi}$ given by equation (4.14). We obtain the potential for the motion of ϕ by integrating the right hand side of equation (4.43) with respect to

ϕ. It corresponds to a horizontal line at a value $\psi = \bar{\psi}$ in figure 4.1. Taking for $\bar{\psi}$ a value in between the two extrema of the curve $\dot{\phi} = 0$, we find that ϕ possesses three stationary solutions. This is depicted in figure 4.3 for two values of the IP_3 concentration. It shows the typical shape of a bistable potential. Thus, all conditions of the previous section are fulfilled.

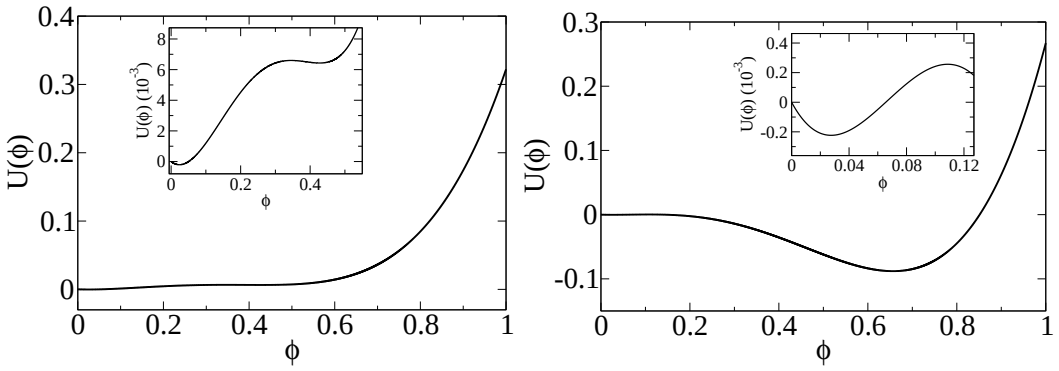

Figure 4.3: Potential $U(\phi)$ for $I = 0.0225\mu M$ (left) and $I = 0.032\mu M$ (right). The left panel shows the potential just before the second saddle node bifurcation. The insets depict an enlarged view for $U(\phi) \approx 0$. Note the difference in scale for the axis. Parameters as in figure 3.6, $d_5 = 0.832\mu$M and $\psi = \bar{\psi}$.

To compute the mean first passage time the values of a and b as well as for the stable fixed point A are needed. In analogy with figure 4.2 we identify A with the left stationary state $(\bar{\phi}, \bar{\psi})$ in figure 4.1. It complies with the stationary state of low Ca^{2+} concentration to which the IP_3 receptors return in between oscillations (Marchant and Parker 2001). The boundary values are obtained differently for the two Fokker-Planck equations. For the nonlinear Fokker-Planck equation they follow from the fixed points of the macroscopic equations. We set $a = 0$ and b to the value $\bar{\phi}_u$ of the instable stationary state. In the case of the linear Fokker-Planck equation for the noise, we go back to equation (4.4a). The requirement $n_{10} \geq 0$ leads to $a = -\Omega^{1/2}\bar{\phi}$. For the right boundary we find $b = (\bar{\phi}_u - \bar{\phi})\Omega^{1/2}$. It reflects that the noise can carry the system only to the barrier at $\bar{\phi}_u$ and not any further. The discrete nature of the master equation demands a mapping of the real boundary values to integer ones. We use the results of the nonlinear Fokker-Planck equation for n_{10}, so that we set $L = 0$ and $R = [\bar{\phi}_u \Omega]$. The notation $[x]$ refers to the integer that is closest to x. Moreover, we assign $m = [\bar{\phi}\Omega]$.

We now calculate the mean first passage time according to equation (4.41) with

$$g_i = \frac{b_6 c(i)}{c(i) + d_5}\bar{q} + (hN - i - \bar{q})a_5 c(i)\,, \quad r_i = b_5 i + a_6 i c(i)\,, \tag{4.44}$$

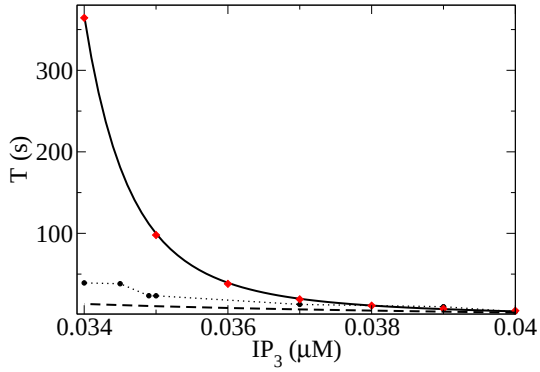

Figure 4.4: Mean first passage time in dependence on I for the Ω expansion (solid), the nonlinear Fokker-Planck equation (dashed) and the master equation (dots). Diamonds represent the variance for the Ω expansion. Parameters as in figure 3.6 and $d_5 = 0.843\mu M, N = 25$.

and $\bar{q} := [\bar{\psi}\Omega]$. Figure 4.4 shows the results in dependence on the IP_3 concentration together with those for the Fokker-Plan equations. For the Ω expansion we apply equations (4.33) and (4.37). The data of the two approaches are indistinguishable. For equation (4.33) we only need the four leading eigenvalues of the expansion (4.30) to achieve this agreement. Whereas solutions of the Fokker-Planck equation are continuous, the master equation possesses discontinuous solutions. This arises from the discreteness of the hopping process. The jumps in the mean first passage time are dominated by the value of the right boundary. Whereas changing the starting point m shows only small effects, increasing the right boundary b induces large jumps in the mean first passage time. In comparison with the master equation the nonlinear Fokker-Planck equation underestimates the mean first passage time, wheres Van Kampen's Ω expansion overestimates it. The nonlinear Fokker-Planck equation proofs as a better approximation. The overrating of the Ω expansion can be attributed to its parabolic character. It describes the noise as a parabola around the stable fixed point. In contrast to the macroscopic potential that possess an inflection point and a maximum for $\phi > \bar{\phi}$, the noise ξ is governed by a strictly increasing function. It is still convex when the macroscopic potential is already concave. This can result in a value too large for the barrier.

Nevertheless the Ω expansion possesses a range where it reasonably approximates the master equation. This is illustrated in figure 4.5. It depicts the mean first passage time for the same parameters as figure 4.4, but with $N = 15$. The inset shows that for some values of the IP_3 concentration the Ω expansion even interpolates the master equation. Yet, with decreasing I, we recover the same

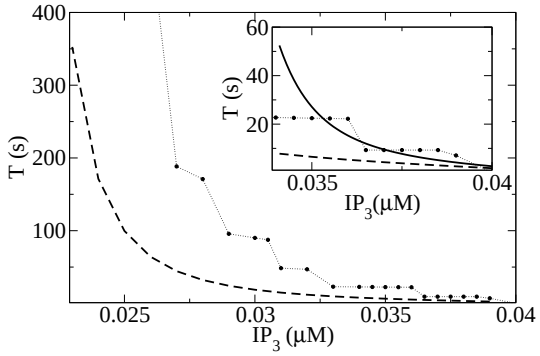

Figure 4.5: Mean first passage time in dependence on I for the Ω expansion (solid), the nonlinear Fokker-Planck equation (dashed) and the master equation (dots). Parameters as in figure 3.6 and $d_5 = 0.843\mu M, N = 15$.

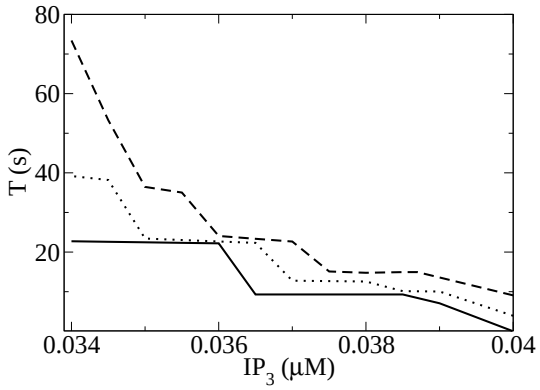

Figure 4.6: Mean first passage time in dependence on I for the master equation for $N = 15$ (solid), $N = 25$ (dotted) and $N = 40$ (dashed). Parameters as in figure 3.6 and $d_5 = 0.843\mu M$.

trends as in figure 4.4. The mean first passage time grows much faster with decreasing I for the Ω expansion than for the two other methods. Therefore, we present data for the master equation and for the nonlinear Fokker-Planck equation in the main plot of figure 4.5 only. The values of T are comparable to frequencies reported earlier for Ca^{2+} puff (Marchant et al. 1999). However, they do not equal the mean first passage time because that latter describes the stochastic part of the puff period only.

The strong increase in the mean first passage time for small IP_3 concentrations originates from the response of the bistable potential $U(\phi)$ to a change in I as figure 4.3 shows. When we lower I, the right minimum moves upward. For concentrations $I > I_c$ the potential at the right minimum is higher than at the

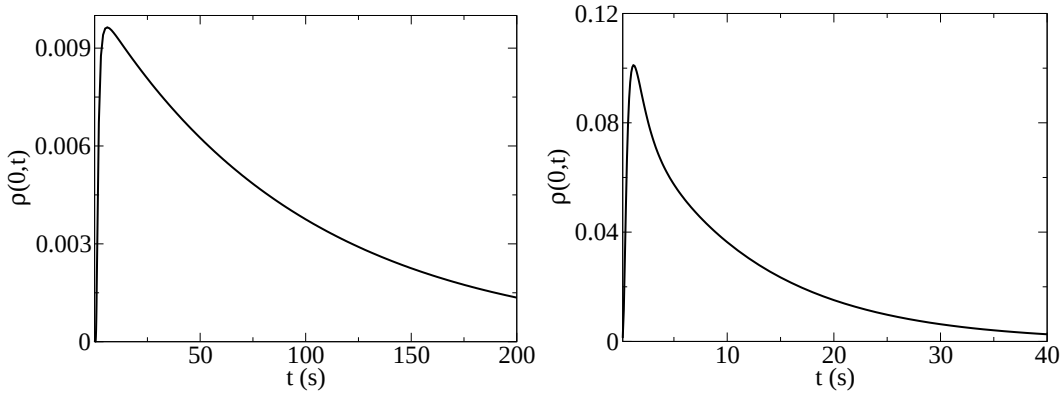

Figure 4.7: Escape probability $\rho(0,t)$ for van Kampen's Ω expansion. Parameters as in figure 4.4 with $I = 0.035\mu M$ (left panel) and $I = 0.038\mu M$ (right panel).

left minimum. Thus, the barrier grows for smaller IP_3 concentrations. Moreover, the ϕ value for the local maximum is shifted to the right which results in a broader left well. This all leads to longer mean first passage times. The left boundary for the IP_3 concentration in figure 4.5 is given by I_m. It is the lowest value of I for which ϕ still possesses a bistable potential. On lowering I the nullcline of ϕ is shifted downward in figure 4.1. Consequently, for all $I < I_m$ the value of the local maximum is smaller than $\bar{\psi}$ so that the bistable regime vanishes via a saddle node bifurcation.

A comparison of figure 4.4 and figure 4.5 brings the dependence of the mean first passage time on the number of channels per cluster forward. A more detailed view is provided in figure 4.6. It shows the mean first passage time computed from the master equation for N=40, 25 and 15. It grows with increasing N. This is readily understood by the role that N plays. When we change N, we keep the maximal radius of the source area fixed. Consequently, each channel occupies less space of the cluster when we increase N. A change in the number of open channels then leads to a smaller variation in the conducting area. This entails smaller fluctuations. As the mean first passage time is driven by fluctuations, it grows with increasing N. Formally, the influence of N can be deduced from equation (4.21). The second derivatives determine the strength of the fluctuations. They scale like $1/N$, so that they become less important for large N. Eventually, the mean first passage time diverges in the limit $N \to \infty$, because a deterministic system never leaves a fixed point. This role of N explains why it is possible for the Ω expansion to give reasonable results for the mean first passage time, although it overestimates the barrier. When fluctuations grow as for $N = 15$ compared to $N = 25$, the overrating of the barrier becomes less important. This can be seen as follows. Suppose the height of barrier is written as $h + \delta h$, where δh is the

error induced by the Ω expansion. The escape time scales as $\exp(h/\epsilon + \delta h/\epsilon)$, where ϵ denotes the strength of the noise. The larger ϵ, the smaller is $\delta h/\epsilon$ and consequently the influence of the error in the barrier on the escape time.

As a last step we apply equation (4.30) to calculate the probability density $\rho(0,t)$, i.e. $\rho(0,t)dt$ is the probability that the system reaches the barrier in the interval t and $t + dt$. Note that the starting point for the escape process is $x = 0$. In the Ω expansion, the Fokker-Planck equation describes the noise only. At $t = 0$ the system is exactly in the macroscopic state A. Hence the noise vanishes at $t = 0$. The results are depicted in figure 4.7. The smooth shape of the curves requires less than 10 eigenvalues. The plots show the well known rising phase of ρ and then the exponential decay. We find a maximal probability ρ_m which is shifted toward shorter times for higher IP_3 concentrations. The same tendency is observed for the mean first passage time in figures 4.4, 4.5 and 4.6. This agrees with the effect of IP_3 on the IP_3 receptors. The higher I, the more excitable they are. Hence the Ca^{2+} concentration grows which entails higher transition rates and shorter mean first passage times.

The probability density ρ allows a direct computation of the variance for the escape process. Whereas the mean first passage time $T = \langle t(x) \rangle$ represents the first moment, the variance σ is obtained from $\sigma^2 = \langle t(x)^2 \rangle - T^2$. The calculation of the variance is computationally cheap, because only one additional integration is needed once the first moment is known. This is a general strength of the Ω expansion. We find any moment of the time with one integration. Moreover, a good convergence of the moments can be obtained with a few eigenvalues only. Six eigenvalues are enough for the variance in this case. The results are shown in figure 4.4. The variance and the mean are almost identical. This hints at the Poissonian character of the escape process.

4.5 Discussion

We have derived a master equation and two Fokker-Planck equations to describe the dynamics of IP_3 mediated Ca^{2+} dynamics. Among the different approaches to approximate a master equation by a Fokker-Planck equation we have chosen van Kampen's Ω expansion and an ansatz based on the Kramers-Moyal expansion. Master equations and corresponding Fokker-Planck equations for intracellular Ca^{2+} have been investigated in the past (Shuai and Jung 2002a, Shuai and Jung 2002b, Meinhold and Schimansky-Geier 2002), but the study at hand is founded on different ideas. Most of the previous works use the Li-Rinzel model (Li and Rinzel 1994) for the dynamics of a single subunit of an IP_3 receptor. It describes the time evolution of the fraction of subunits that are not inhibited

yet, taking advantage of the time scale separation between IP_3 activation, Ca^{2+} activation and Ca^{2+} inhibition. We employ a state scheme for one subunit that only eliminates the IP_3 dynamics adiabatically. We keep the activating Ca^{2+} and inhibiting Ca^{2+} dynamics. From the resulting 4 states we lump the inhibited states to a single state. It results in a three state model for one subunit. This state scheme allows to track the transition $110 \leftrightarrow 100$. It is essential for the number of activated subunits and therefore the Ca^{2+} concentration. Moreover, the separation of time scales between Ca^{2+} activation and Ca^{2+} inhibition does not necessarily always hold.

All master equations that have been studied by now describe the number of active subunits of the IP_3 receptors. However, the mere number of active subunits does not uniquely determine the number of open channels and thus the Ca^{2+} concentration. The latter is necessary for the transition rates. A given number of active subunits leads to a varying number of open channels as figure A.1 shows. We have therefore computed the distribution function of open channels when the number of active subunits is known. It turns out that it is sharply peaked and that the number of open channels is well characterized by the average. We use it in the model of section 3.4 to compute the Ca^{2+} concentration profiles. We set the radius of the source area proportional to the fraction of open channels determined by this average. For the Fokker-Planck equations the fraction of open channels is determined by the macroscopic fraction of open subunits p_{110}. Taking the continuous limit of the averages in equation (A.15) and (A.14) reproduces these fractions. Thus we see how the macroscopic equations consistently evolve from the microscopic view of the master equations.

In a second step we used the master equation and the Fokker-Planck equations to compute the mean first passage time from the stationary state of low Ca^{2+} concentration. To this aim we reduced the two dimensional equations to one variable. In contrast to the equations in (Shuai and Jung 2002a, Shuai and Jung 2002b, Meinhold and Schimansky-Geier 2002) we keep the fast variable. On the time scale on which the number of activable subunits n_{10} changes, the number of inhibited subunits $n_{\bar{h}}$ remains constant. Another difference to the above models lies in the applied Ca^{2+} concentrations. The above authors employ the parameters of the original DK model. It was set up for averaged Ca^{2+} concentrations which are much smaller than those at an open cluster. The binding rate constant for Ca^{2+} activation and Ca^{2+} inhibition are therefore overestimated in the DK model, whereas the dissociation constants are too small. We used the parameters of chapter 2 which reflect the large Ca^{2+} concentrations at an open cluster.

The discreteness of the master equation admits to follow the number of open channels during the escape process. For the chosen parameters we find that not

a single channel opens during this time. The Ca^{2+} concentration stays just above base level. If one channel had opened the Ca^{2+} concentration would have risen up to more than $20\mu M$ at the cluster. This result sheds new light on the stochastic fraction of the puff period. It seems that the nucleation of open channels is not the determining factor. On the contrary the stochastic contribution happens before the first channel opens. Even if we set the Ca^{2+} concentration to base level for the whole escape process the system still reaches the barrier. It only takes longer. The reason why the Ca^{2+} concentration is not identical to the base level although no channel is open stems from the average in equation (A.14). We will investigate this phenomenon more closely in the future.

For the master equation as well as for the Ω expansion the mean first passage time can be computed analytically. A comparison of the Fokker-Planck equations with the master equation reveals that the Ω expansion overestimates it and the nonlinear Fokker-Planck equation underestimates it. Yet, the latter represents a better approximation to the master equation, although for some values of the IP_3 concentration, the Ω expansion approaches the master equation very well. From a computational point of view the Ω expansion possesses some advantages. Any moment of t is obtained from one integration which is easily performed. The nonlinear Fokker-Planck equation requires the solution of a set of differential equations. To calculate the nth moment, n equations must be solved.

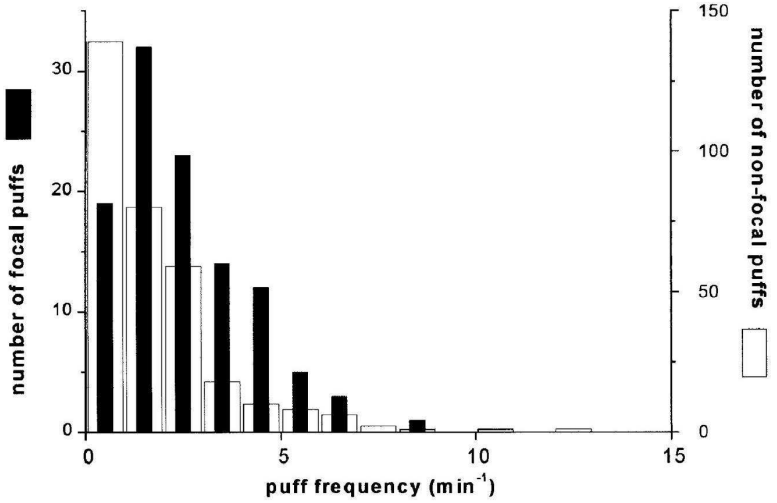

Figure 4.8: Frequencies of puffs from focal sites (filled bars) and from non-focal sites (empty bars). A focal site corresponds to an area of increased cluster density compared to non-focal sites. The inter cluster distance is smaller in a focal site than in a non-focal site. Figure from (Marchant and Parker 2001).

These mean first passage times can be associated with experimentally observed puff frequencies. The results in figure 4.5 are close to measured values as shown in figure 4.8. However, the puff frequencies do not correspond to the mean first passage times. The latter represent only a part of the periods because they describe the processes after recovery from inhibition.

The drawback of the above method is the limitation to one variable. To tap the full potential of equation (4.1) different methods are needed. An interesting approach in this direction has been proposed by Henry et al., (Henry and Levine 2003). They use a path integral formalism coupled to a minimization procedure. It will be interesting to see what the influence of a second dimension in the escape process is. A thorough study of these different approaches can therefore be a forward step in understanding the fundamental processes of intracellular Ca^{2+} dynamics.